A deep look into the diverse surface speciation of the mono-molybdate/lepidocrocite system by ATR-IR and polarized ATR-IR spectroscopy

Romain Botella, Grégory Lefèvre

A deep look into the diverse surface speciation of the mono-molybdate/lepidocrocite system by ATR-IR and polarized ATR-IR spectroscopy

*Romain Botella and Grégory Lefèvre**

PSL Research University, Chimie ParisTech-CNRS, Institut de Recherche de Chimie Paris, 11 rue Pierre et Marie Curie, F-75005 Paris, France

* Corresponding author: gregory.lefevre@chimieparistech.psl.eu

Abstract

The present study is focused on the adsorption of monomeric molybdate anions on the surface of lepidocrocite investigated by several infrared spectroscopy methods. To study the surface speciation of molybdates on lepidocrocite, the behavior of the anion at the interface upon increasing anion concentration (fixed pH) or decreasing pH (fixed concentration) was analyzed in situ. The obtained results expand the knowledge for surface speciation by revealing a second molybdate complex, which is more stable, arising from the interaction with defects on the (010) facets of lepidocrocite. A curve fitting procedure enabled us to confirm what is observed from the pristine spectra, and outer-sphere complexes were probed as well. The evolution of the different bands upon increasing adsorbate concentration and decreasing pH, as obtained by curve fitting, shows a complex evolution for the different surface species with protonation, with the formation of strongly bonded complexes at low pH. The 2D synchronous and asynchronous spectra support the interpretation of the data. Furthermore, insights into the orientation of the complexes with respect to the lepidocrocite surface are obtained by using linearly polarized radiation. The results confirm most of the conclusions ascertained on the basis of the unpolarized spectra. The combination of the different methodologies yields a consistent picture for the complexity of this system and paves the way for subsequent utilization of this approach to study other systems.

Keywords: molybdenum, iron hydroxide, vibrational spectroscopy, linear dichroism, surface rearrangement, anisotropy

1. Introduction

Oxoanion adsorption on metal oxides is an important phenomenon in several research domains, such as heterogeneous catalysis and geochemistry. One way to study adsorption mechanisms is to use in situ infrared (IR) spectroscopy in attenuated total reflectance (ATR) mode [1]. Such spectroscopy enables us to hone the surface speciation of these oxoanions, which is indirectly obtained by macroscopic methods [2,3]. Numerous studies of oxoanions using such techniques have been published (e.g., sulfates [4] or selenates [5]), as other ions, such as molybdates and tungstates, have been less studied. However, these anions are worthy of interest due to their peculiar behavior; they can polymerize, which impacts their reactivity in heterogeneous catalysis [6] or ecotoxicology [7]. Their presence and distribution in soils are also an active research subject, as molybdates can be both essential nutrients and pollutants for soils [8]. In relation to this pollution capacity, their adsorption on ferric (hydr)oxides [9, 10] can shed light on how an excess in molybdate soil can be remediated.

IR spectroscopy provides much information for surface species [11], but one characteristic that remains elusive with this technique (as well as with other usual spectroscopies) is the orientation of the adsorbate on a surface. This predicament can be lifted by combining the use of polarized IR radiation and an anisotropic substrate. The adsorbate can in turn share such anisotropy, and the use of polarized IR light can lead to direct knowledge of how anions are located at the surface. Polarized ATR-IR has already been used to study Langmuir-Blodgett films [12] or to measure the organization degree and orientation of solid deposits by measuring the respective orientation of one substrate deposited at another material surface [13]. The geometry of the adsorbate itself has been evaluated in a few articles [14,15]. To apply this approach to molybdate adsorption, an anisotropic substrate is mandatory. Lepidocrocite is an iron oxyhydroxide that can be synthesized as lath-shaped

72 nanoparticles [16]. An anisotropic nanoparticle film suitable for use in polarized ATR-IR
73 spectroscopy can be prepared by depositing these particles on a flat surface, such as an ATR
74 crystal.

75 In solution, the molybdate ion geometry can change depending on the pH: the MoO_4^{2-} anion
76 is stable as a tetrahedral (T_d) geometry, solvated by four water molecules. The protonated
77 forms $HMoO_4^-$ and H_2MoO_4 tend to have its Mo center solvated by two more water molecules
78 and to become octahedral (O_h) [17]. DFT calculations have shown [14] that the octahedral
79 geometry is unstable for the surface complex and that the molybdates are adsorbed with a
80 tetrahedral geometry on the lepidocrocite surface, regardless of the degree of protonation.
81 Moreover, molybdates can polymerize in solution, but previous work on such a reaction at the
82 iron (hydr)oxide/aqueous solution interface has suggested that polymolybdates are not
83 chemically stable on the surface of lepidocrocite [15]. Other works for other metal oxide
84 surfaces, such as titanium dioxide or alumina, indicate that the polyanion can only be
85 reversibly adsorbed (as outer-sphere complexes) [6]. As a first step, to avoid the complexity
86 of having polymolybdate in solution and/or close to the surface, we studied the system with
87 chemical conditions for which polymolybdates are not formed in solution.

88 The molybdate/lepidocrocite system has been previously studied [14,15] using ATR-IR and
89 DFT calculations. The authors managed to sketch the broad outlines of the surface speciation
90 and to use polarized ATR-IR as proof of the application of the technique to the system. In the
91 present work, a more complete grasp of the surface speciation of molybdates on lepidocrocite
92 is obtained thanks to the analysis of a higher wavenumber range and the extensive use of
93 polarized ATR-IR following optimization of the experimental protocol.
94
95

2. Materials and methods

2.1. Materials

All solutions and suspensions in the aqueous phase were prepared using purified water (Milli-Q, Millipore) with a resistivity of 18.2 MΩ·cm. An aqueous molybdate solution (0.1 M) was prepared from $Na_2MoO_4 \cdot 2H_2O$ (Prolabo). In the sample solutions, the ionic strength was fixed at 0.01 M NaCl salt (VWR Prolabo). Acidification was performed with a 1 M HCl solution (Fischer Scientific). Lepidocrocite with a N_2 Brunauer−Emmett−Teller (BET) surface area of 76 m^2/g was synthesized in two steps according to the protocol of Schwertmann and Cornell [18] based on the hydrolysis of an iron(II) salt followed by oxidation of the obtained precipitate by controlling the pH and kinetics.

2.2. In Situ ATR-IR Spectroscopy

The ATR-FTIR spectra were collected with a dry-air-purged Thermo Scientific Nicolet 6700 FT-IR equipped with an MCT (Mercury-Cadmium-Telluride) detector. The spectral resolution was 4 cm^{-1}, and the spectra were averaged from 256 scans. The horizontal ZnSe crystal with a single reflection (A = 2.54 mm^2) and an angle of incidence of 45° (Smart PIKE) was coated with 1 µL of the lepidocrocite suspension (1 g/L), which was dried under a flow of N_2. This procedure was repeated three times. The flow cell was placed onto the ATR accessory, and a background spectrum was recorded when the initial solution (0.01 M NaCl) reached the oxide film for conditioning, with a constant flow rate of 1 mL/min achieved using a peristaltic pump (Ismatec S.A.) at room temperature. During the hydration step, spectra were taken every ten minutes. When the subtraction of two consecutive spectra gave a similar

spectrum to that of the baseline, a second background spectrum for the hydrated film was recorded. Then, a given volume of a 0.1 M sodium molybdate stock solution was added to the circulating solution. The evolution of molybdate sorption onto lepidocrocite was monitored by the acquisition of spectra in minute steps. Using the same stability criterion, when the subtraction of two consecutive spectra gave a similar spectrum to that of the baseline, a stationary state was assumed to be reached. Approximately 20−30 min was required after each experimental change (pH or concentration). The pH was adjusted with HCl and recorded using a pH meter (Metrohm). OMNIC software was used for data reprocessing, and spectra were decomposed with Gaussian peaks and a spline baseline by interpolation using OriginPro 8.6 software. The fitting procedure was performed until the coefficient R^2 was equal to 0.99, and decomposition was achieved with the minimum number of peaks for the fitted areas, wavenumbers, and widths.

To collect polarized ATR-FTIR spectra, a ZnSe manual polarizer (Pike Technologies) was placed between the light source and ATR accessory to select the polarization of the IR beam. The signal was divided into two components with either p-polarized light or s-polarized light to collect A_p and A_s spectra, respectively. Since the incident angle of the IR beam to the IR is 45°, s-polarization corresponds to the direction of the y-axis of the Cartesian coordinate system, and, therefore, is parallel to the crystal surface, while the polarization is in the xy-plane, perpendicular to the crystal surface, and therefore contains vibrational modes both parallel and perpendicular to the crystal. It is possible to obtain the polarized spectra direction along the three Cartesian directions (A_x, A_y, and A_z) by using the following equations [19, 20]:

$$A_z = A_p - kA_s \qquad (1)$$

$$A_s = A_y \quad (2)$$

$$A_p = A_x + A_z \quad (3)$$

where the factor k varies according to the nature of the crystal and the incidence angle. For a ZnSe crystal with an incident angle of 45°, k = 0.791. As the spectra for A_s and A_p show distributed baselines, a manual correction of the baseline was carried out for four points chosen in the unpolarized spectra (minima between bands). The systematic choice of these points enabled rigorous correction while producing small aberrations for some of the spectra.

2D correlation spectra were calculated with the free software 2Dshige [21] with the dynamic spectra mode (the average spectrum was subtracted from the whole series for each sample spectrum [22]). An automatic baseline was subtracted before this mathematical treatment using OMNIC software.

2.3. Computational method

The DFT calculations were carried out by using an ab initio plane-wave pseudopotential approach as implemented in VASP [23,24]. We used the DFT+U approach, with the Perdew−Burke−Ernzerhof (PBE) functional [25], a projected augmented wave (PAW) basis set, and the generalized gradient approximation (GGA), and included van der Waals forces at the D2 level [26]. The DFT+U method has already been used in the literature to study iron oxides such as magnetite [27], hematite [27, 28], and goethite [27, 28]. After parameter optimization, Ueff = 5 eV was found to be the best value to reproduce both the band gap [27] and the cell dimensions of bulk FeOOH [29]. An energy cutoff of 400 eV for the plane-wave

basis set was used. For the bulk optimization, the integration of the Brillouin zone was performed using k points of (6 × 2 × 8). Geometry optimizations were performed with a convergence threshold of 10^{-4} eV/cell. Only bulk lepidocrocite has been optimized and its vibrational spectrum has been simulated. In the dipolar approximation, the intensity of the band ω is defined as follows [30]:

$$I(\omega) = \sum_{\alpha}^{3} | \sum_{\beta}^{3} \sum_{l=1}^{M} Z^{*}_{\alpha\beta}(l) e_{\beta}(l)|^{2} \qquad (4)$$

where α and β are Cartesian coordinates, e(l) is the vibrational eigenvector of the l^{th} atom and $Z^{*}_{\alpha\beta}(l)$ is the effective Born charge tensor for the l^{th} atom. The A_z and A_y components of absorbance were obtained from the data computed during the IR calculations. These components correspond to the members of (4) with the squared component of the atomic movement for the corresponding mode as a common factor.

3. Results and discussion

3.1. Evolution of the surface speciation with concentration

First, the adsorption of the dianion MoO_4^{2-} was performed. At pH 8, the geometry of the ion is tetrahedral; hence, no geometric change is expected during adsorption. The range of low concentrations used, as well as the high pH value of the solution, enables only the dianion to be present in solution as well as at the surface. The results obtained for increasing concentration are shown in Figure 1. In solution, molybdate ions are characterized by only one band at approximately 833 cm^{-1}, corresponding to the degenerated asymmetric stretching of the Mo-O bonds (ν_3 band, Figure 1A) [31,32]. In the adsorbed state, the spectrum consists

196 of three or four bands (e.g., 919 cm^{-1}, 864 cm^{-1} and 748 cm^{-1}) due to the evolution of its

symmetry when adsorbed on lepidocrocite [15,31]. The first band is associated with a

symmetric stretching of the Mo-O bonds (ν_1 band), and the two other bands are associated with asymmetric stretching (ν_3 bands). An oxoanion can adsorb at the surface of a metal hydroxide with several adsorption modes, as depicted in Figure 1A: either it bonds to the surface with one of its oxygens (one vertex of the tetrahedron in Figure 1A), forming a monodentate surface complex, or it bonds with two oxygens (one edge of the tetrahedron) to form a bidentate complex. Each of these species can interact with one (monodentate) or two (bidentate) surface sites. Monodentate and bidentate adsorption modes have different IR spectra, as shown in Figure 1A. These surface complexes are called inner-sphere complexes, as opposed to outer-sphere (OS) complexes that consist of ions physically interacting with the surface (electrostatic interactions or hydrogen bonds). They maintain the same symmetry as the free ions in solution; hence, only one IR band is expected to be observed in their spectrum.

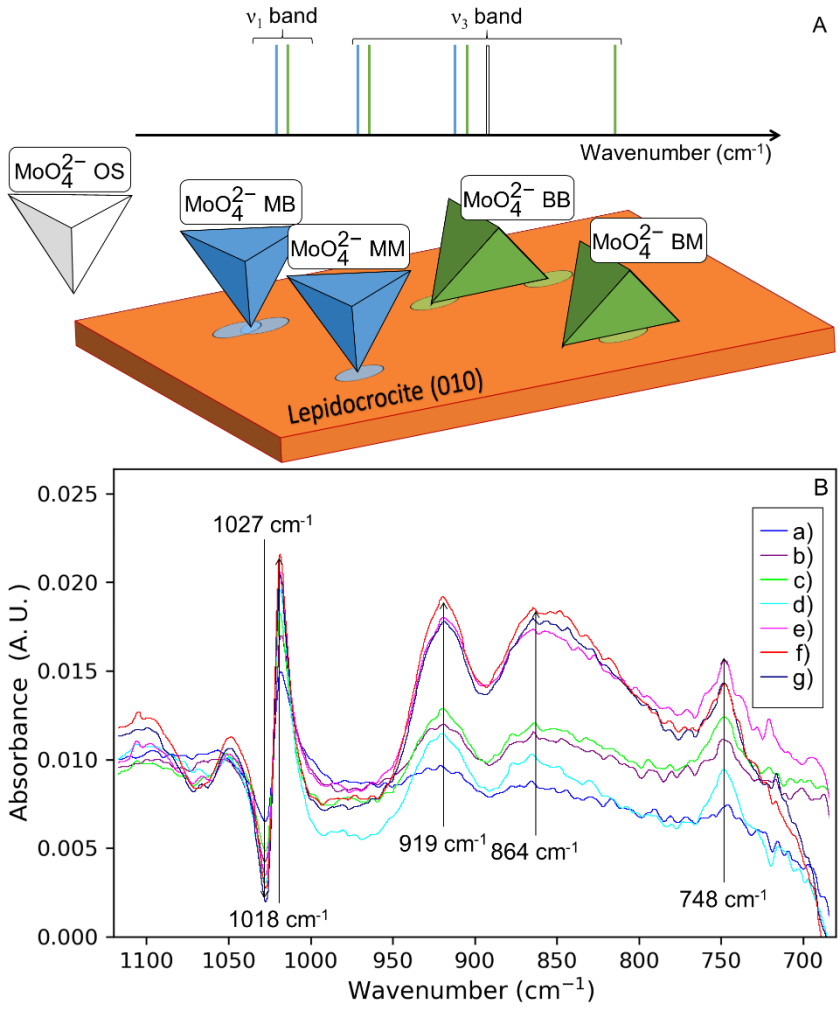

Figure 1. Diagram of the different surface complexes that can be produced from the adsorption of an oxoanion such as molybdate at a surface and their associated IR spectra. The blue complexes correspond to monodentate species (MB: monodentate binuclear and MM: monodentate mononuclear), and the green complexes represent bidentate species (BB: bidentate binuclear and BM: bidentate mononuclear). The white tetrahedron represents the outer-sphere (OS) complexes mentioned in the main text. The spots represent the number of surface sites involved in the adsorption mode (A). Spectra measured for the lepidocrocite/molybdate system with increasing adsorbate concentration at pH 8 (B): a) 1.10^{-5} $mol.L^{-1}$, b) 4.10^{-5} $mol.L^{-1}$, c) 8.10^{-5} $mol.L^{-1}$, d) 1.10^{-4} $mol.L^{-1}$, e) 4.10^{-4} $mol.L^{-1}$, f) 8.10^{-4} $mol.L^{-1}$, g) 1.10^{-3} $mol.L^{-1}$.

In the presence of solids, it should be noted that the spectral signal arises only from the surface and not from the solution due to the low sensitivity of ATR-IR toward aqueous species. Previous work on the same system has not mentioned the band at 748 cm^{-1}, perhaps due to instrument limitations. The band at 864 cm^{-1} shows a marked asymmetry, which might arise from the overlap of several components. According to the literature [31,33], the band at 919 cm^{-1} corresponds to the symmetric stretching modes of Mo-O bonds for the adsorbed ion and confirms the chemisorption of molybdates on the substrate surface.

The simplest surface complex on lepidocrocite regarding molybdates is the binuclear monodentate complex on the (010) face. For simplification, the binuclear geometry will be assumed for both monodentate and bidentate unless stated otherwise. A previous spectroscopic study with experimental spectra and DFT calculations ascertained that this type of inner-sphere complex is dominant in this system [31] and is characterized by two bands in the wavenumber range of 950-850 cm^{-1}. Another possible adsorption mode is a bidentate complex. Its symmetry is lower than that of the previous complex, which leads to the splitting

234 of the asymmetric stretching of Mo-O bonds, associated with the appearance of a new band in
235 the spectrum (Figure 1A) in the wavenumber range of the molybdate species (between 1000
236 cm^{-1} and 700 cm^{-1}). Such a complex on the surface of hematite, another ferric oxide, should
237 show a supplementary band at approximately 782 cm^{-1} according to DFT calculations [34].
238 Both of these features are found in Figure 1B. It should be noted that another origin for the
239 band at 748 cm^{-1} could be the formation of a hydroxyl group, whose wavenumber in
240 lepidocrocite lies in this range. However, this possibility is ruled out since the coadsorption of
241 a hydroxide ion or the protonation of a surface hydroxyl group along with the adsorption of a
242 molybdate ion is unlikely.
243

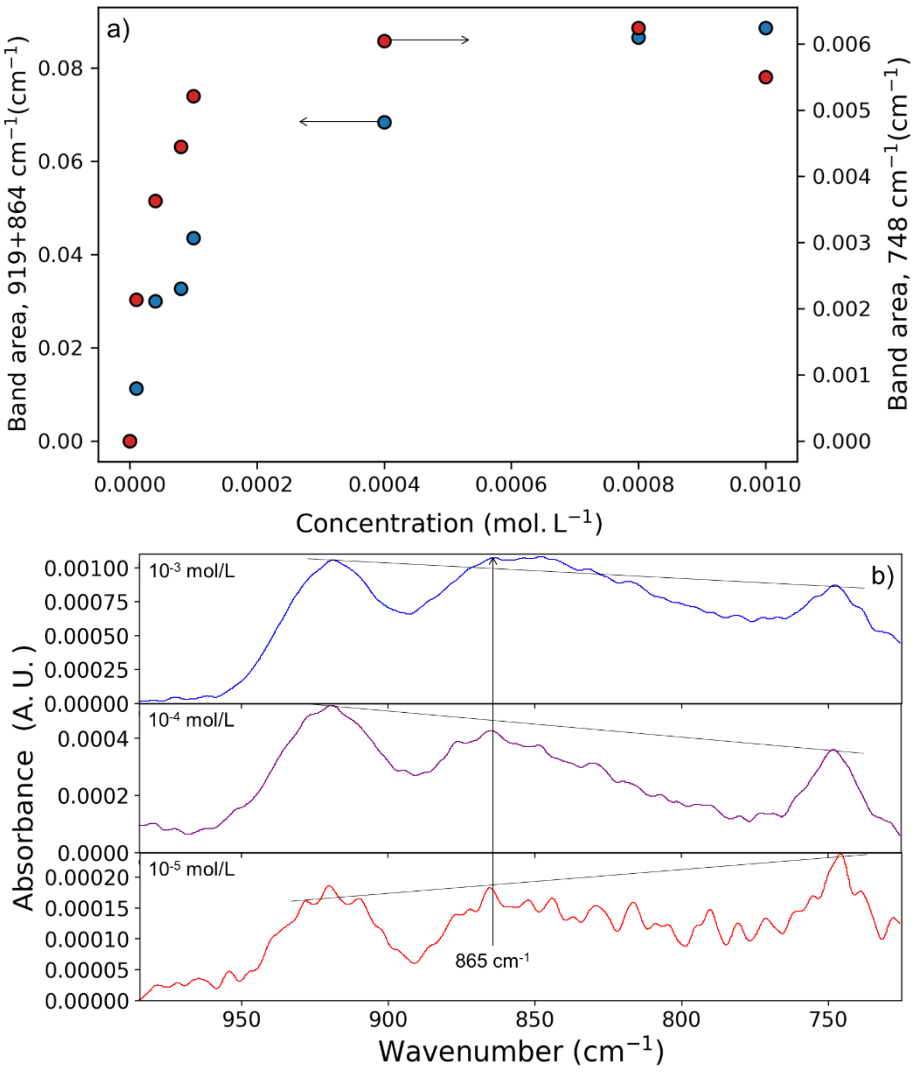
a)
Band area, 919+864 cm^{-1}(cm^{-1})
Band area, 748 cm^{-1}(cm^{-1})
Concentration (mol. L^{-1})
b)
10^{-3} mol/L
10^{-4} mol/L
10^{-5} mol/L
865 cm^{-1}
Absorbance (A. U.)
Wavenumber (cm^{-1})

244

245

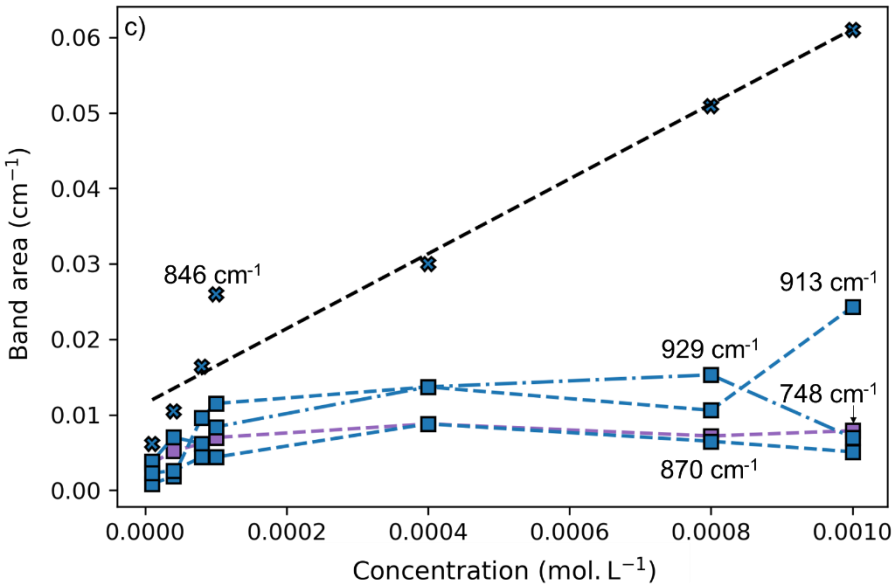

Figure 2: a) Band area evolution for the 919+864 cm^{-1} band cluster (left axis) and the 748 cm^{-1} band (right axis) as a function of molybdate concentration. b) Comparison of the intensity of the major spectral bands for an adsorbate concentration of 10^{-5} mol. L^{-1} (red), 10^{-4} mol. L^{-1} (purple) and 10^{-3} mol. L^{-1} (blue). c) Band area evolution for the signals separated after curve fitting. The black dashed line in b) is a guide to the eye, as the black lines in c) enable us to observe the stronger intensity of the 919 cm^{-1} and 748 cm^{-1} bands with respect to the 865 cm^{-1} band.

From a quantitative point of view, the areas for the bands between 970 cm^{-1} and 775 cm^{-1} and for the 750 cm^{-1} band are shown in Figure 2a. These areas evolve in the same way as the molybdate concentration in aqueous solution and resemble a type I isotherm [35] or Langmuir isotherm [36]. However, the evolution does not fully overlap, suggesting that these bands originate from different surface species. This observation is confirmed by a comparison of the spectra measured for different adsorbate concentrations over two orders of magnitude (Figure 2b), which shows an evolution of the relative intensity for the different bands.

Another interesting feature is the doublet of bands, one negative and another positive, observed in the wavenumber range of 1050 cm^{-1} to 1000 cm^{-1}, which is narrower than that for the other bands. The negative band comes from the decrease of the intensity at a given wavenumber of a signal present in the background spectrum, while the positive band corresponds to a new signal (or its increase) coming from the modification of the chemical conditions. These wavenumbers are associated with the bending mode of bulk hydroxyls of lepidocrocite [37,38]. Since the molybdate ions are not expected to intercalate between the FeO(OH) layers, those OH moieties must belong to the substrate surface. This feature (sequential negative-positive bands) results from a redshift of the band initially present in the background spectrum, corresponding to the layer of lepidocrocite particles in the presence of solution. This is indirect evidence for molybdate chemisorption at the lepidocrocite surface. The identification of the vibration mode helps to ascertain the prevailing faces where adsorption takes place. The lepidocrocite particles therein are lath-shaped [15,39], and the 1025 cm^{-1} band corresponds to a coplanar deformation of a surface hydroxyl group on the (010) faces. The molybdate ions are, therefore, predominantly chemisorbed on these facets, where they disturb the surface hydrogen bond network around the surface hydroxyls, leading to a decrease in the wavenumber of the vibration by a few cm^{-1}. The increase in the molybdate concentration leads to an increase in the signal intensity but without a further shift. This indicates that the molybdate surface speciation remains the same over the whole range of concentrations studied (10^{-5} to 10^{-3} mol/L).

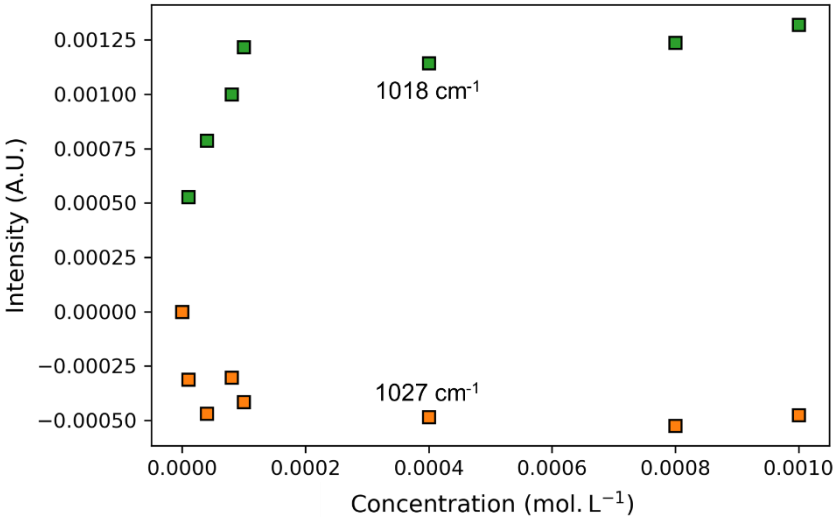

281

282

283 Figure 3: Evolution of the intensity of the positive (green squares) and negative (orange
284 squares) compound of the doublet as a function of the molybdate concentration.

285

286 The evolution of the intensity for each of these bands against the molybdate
287 concentration is shown in Figure 3. The positive component (1018 cm^{-1}) is similar to the
288 evolution of the molybdate bands (Figure 2a)). The negative band (1027 cm^{-1}) is
289 anticorrelated with the other component, with a lower intensity. This analogy for the evolution
290 of both hydroxyl bands of the doublet and the adsorbed molybdate signals supports the
291 existence of a relationship between the two.

292

293 The assignment of the 748 cm^{-1} band is not trivial, all the more as the DFT calculations
294 whose results are given in the literature do not show any bands at this wavenumber for
295 monodentate or bidentate complexes. However, these calculations were only performed for
296 the prevailing face of lepidocrocite, namely, the (010) face. This face is also considered
297 almost nonreactive for a well-crystallized surface according to the surface complexation

MUSIC model [39]. Thus, the observed reactivity can be attributed to the presence of surface defects, whose density should be high enough to produce a roughness at the (010) face according to several works [16,39]. The simulated faces in the calculations of [31] were built from the bulk solid phase (ideal) according to a standard slab formation procedure; hence, the adsorption sites arising from surface defects are absent from such a molecular model. Since defects are expected to be more reactive, molybdates are likely to preferentially adsorbed on these sites before coordinating to other more typical sites (non-defective surface, similar to the one studied by DFT calculations). This is in agreement with the high intensity of the band observed for low adsorbate concentrations (10^{-5} mol/L, Figure 2.b)). Moreover, the interaction energy between molybdate ions and these surface sites is expected to be higher than that characterizing the site of the perfect surface. Thus, compared to the ν_3 band splitting found in the literature [40], the splitting value can be higher in this case [31]. This is consistent with the splitting value calculated between one of the ν_3 bands (overlapped with the ν_1 band [33]) and this band, i.e., $\Delta\nu \approx 165$ cm^{-1}. This ν_3 band splitting is higher than the second band ($\Delta\nu \approx 64$ cm^{-1}, taking the 865 cm^{-1} band as a ν_3 band), which corresponds to the major surface species proposed in the literature [31].

The plateau for both band clusters in Figure 2a) is not reached at the same concentration: the intensity of the band at 748 cm^{-1} is observed to reach a plateau at a lower adsorbate concentration. This is also in agreement with sites defined as surface defects, more reactive and with an expected lower density, which are already saturated while the “classical” sites are not.

To further characterize the surface complexes, a curve fitting procedure was performed for the raw spectra, allowing us to compare the band areas of the different components. The

bands identified in this experiment, as well as during the pH evolution, are summarized in Table 1. As shown in Figure 2c), the bands assigned to the inner-sphere complexes (929 cm^{-1}, 913 cm^{-1}, 870 cm^{-1} and 748 cm^{-1}) vary in a similar fashion to those observed from the pristine spectra shown in Figure 2a): the shape of the curve is similar to a type I isotherm and the fact that the bands reach a plateau for relatively low molybdate concentrations (between 8.10^{-5} and 10^{-4} mol. L^{-1}) may correspond to surface saturation at this pH. A low surface coverage can be associated with a low surface complexation constant at the corresponding pH value. Assuming a uniform surface coverage on the (010) faces of lepidocrocite, this would indicate that adsorbed molecules are located far from each other, which is consistent with the low shift of isolated band wavenumbers observed throughout the adsorbate concentration range. The band at 846 cm^{-1} behaves differently, with a linear increase observed for increasing adsorbate concentration, which agrees with nonspecific adsorption [41] characterizing an outer-sphere complex. Moreover, this assignment is in agreement with the value of the wavenumber, which is close to that of the anion in solution.

Table 1: Summary of the different bands isolated in this work, the pH values are which they appear (X in the column) and their corresponding vibration mode and assignment.

Wavenumber (cm^{-1})	pH			Mode, assignment
	4	6	8	
950	X			ν_1, B
929	X	X	X	ν_1, M
913	X	X	X	ν_3, M
878	X	X		ν_3, HOS
870			X	ν_3, M
846	X	X	X	ν_3, OS
794	X	X		ν_3, B

766	X	X		ν_3, HM
748			X	ν_3, dfMM
736	X	X		ν_3, dfMM
723	X			ν_3, B
707	X	X		ν_3, dfMM

340

341 HOS: protonated outer-sphere complex; HM: protonated monodentate complex

342

343 **3.2. Evolution of the surface speciation with pH**

344

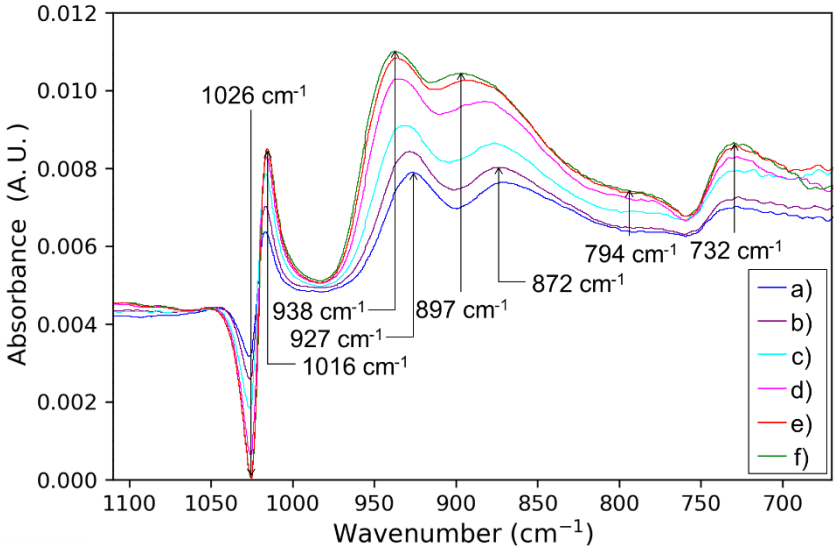

345

346 Figure 4. Spectra measured for the lepidocrocite/molybdate system with decreasing pH and

347 Mo 10^{-4} mol.L^{-1}: a) pH 6.0, b) pH 5.5, c) pH 5.0, d) pH 4.5, e) pH 4.0, f) pH 3.5.

348

349 The study of the molybdate/lepidocrocite system was also performed at a constant

350 molybdate concentration (10^{-4} mol. L^{-1}) and decreasing pH (from 6 to 3.5). This enabled us to

351 observe the behavior of the molybdates for increasing surface charge of lepidocrocite (point

352 of zero charge of lepidocrocite is located at ca. 7-8 [42,43]). Figure 4 shows the spectral

353 evolution with decreasing pH: the intensities of the bands located at approximately 927 cm^{-1}

and 872 cm^{-1} increase, while a shift toward higher wavenumbers is observed. This feature can arise from two behaviors: a shift of the bands or a change in relative concentrations for a limited set of surface complexes, resulting in a shift of the mean value for the wavenumber of the maximum intensity. Several works in the literature have shown that 2D correlation analysis [44] can be used to distinguish between these different behaviors. The result of the analysis of the series is shown in Figure 5. The presence of positive cross-peaks in the synchronous 2D spectrum confirms the growth of bands at (946 cm^{-1}, 897 cm^{-1}), (946 cm^{-1}, 734 cm^{-1}) and (900 cm^{-1}, 731 cm^{-1}). Along with the absence of peaks at these locations in the asynchronous spectrum, these features can be interpreted as being correlated, i.e., either because they belong to the same complex or because they are affected by the pH decrease in the same way. The shape of the peaks in the asynchronous spectrum can be used to find the origin of the intensity shift observed in Figure 5b. For the case of a band shift, a typical kidney shape [22] should be observed, which is not the case for our spectrum. As a consequence, the evolution of the spectra with increasing pH can arise from the evolution of the intensity of several peaks whose wavenumbers do not evolve with pH. A further interpretation of the 2D asynchronous spectrum can allow us to obtain more information about the sequential order of the band evolution [44], but this approach has been questioned for the case of adsorption reactions (without competitive aspect between several adsorbates) [45] and has not been further developed in this work.

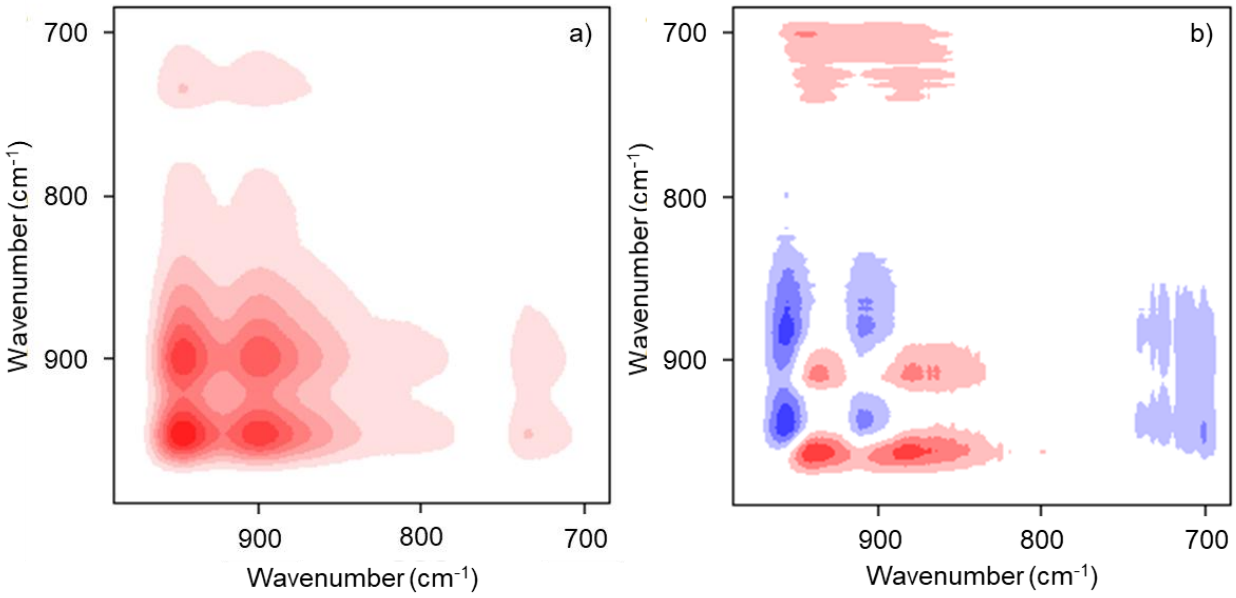

374 Figure 5. (a) Synchronous and (b) asynchronous 2D spectra for molybdate/lepidocrocite at

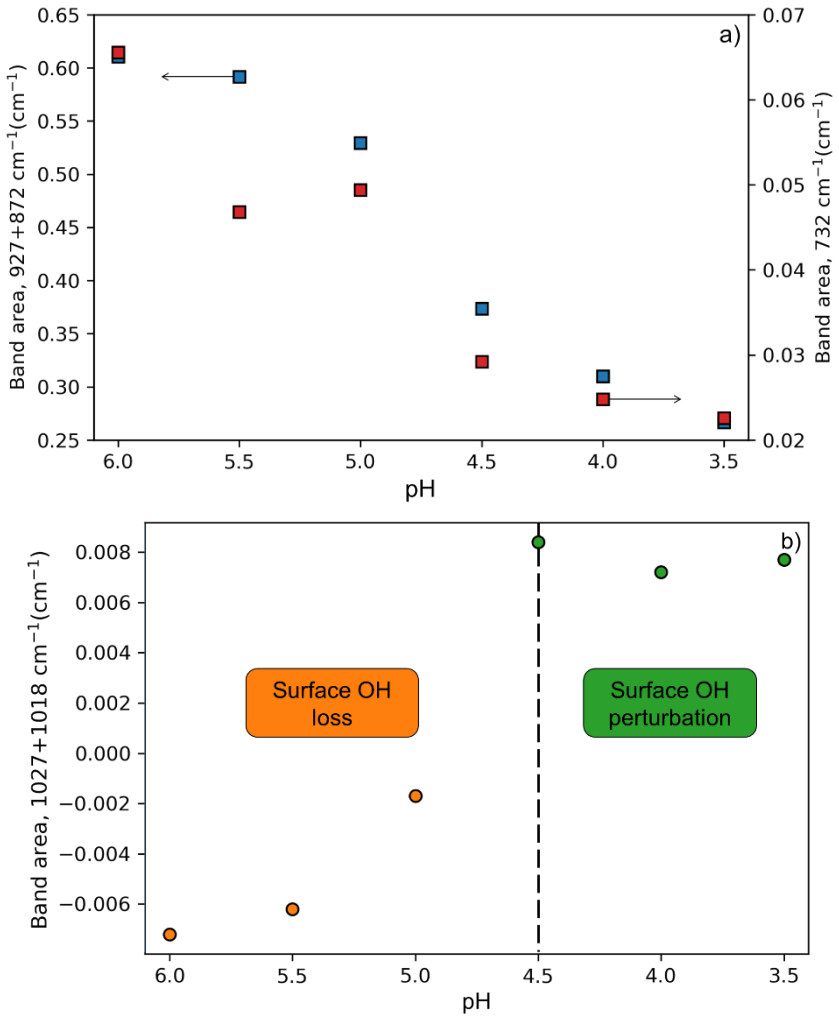

375 different pH values (from 6.0 to 3.5).

376
377

378 Figure 6: Band area evolution with pH for the a) 927+872 cm^{-1} band cluster (left axis) and
379 732 cm^{-1} band cluster (right axis), b) 1027+1018 cm^{-1} band doublet.

380

381 Comparing Figures 1b and 4, it is clear that the pH modification is responsible for the
382 change in the band morphologies. The band assignments are similar to that realized for Figure
383 1b) with the 927 cm^{-1} band (pH 6), corresponding to the symmetric stretching mode of the
384 Mo-O bonds, as assigned in the literature with the help of DFT calculations [31]; the 872 cm^{-1}
385 band (pH 6) arises from the asymmetric stretching of Mo-O bonds and the 732 cm^{-1} band is
386 assigned to the asymmetric stretching of Mo-O bonds of a monodentate complex interacting
387 with the second surface site, in agreement with the previously revealed speciation. The
388 difference between the concentration increase and pH decrease is that some new bands appear
389 for the latter. These new bands arise from the formation of new inner-sphere complexes.
390 Thus, bidentate complexes can be formed since the increase in proton concentration forms
391 surface leaving groups upon adsorption on hydroxyl groups. Monodentate complexes can also
392 be protonated, yielding a $HMoO_4$ surface complex, as suggested in the literature [31].

393 Quantitatively, the area of the 927 cm^{-1} and 872 cm^{-1} bands increases with decreasing
394 pH, with an S-shaped curve observed, as shown in Figure 6a. The area of the band cluster at
395 approximately 732 cm^{-1} increases with decreasing pH.

396 Regarding the surface hydroxyls, the band area for the doublet is plotted in Figure 6b. It
397 follows two successive trends: from pH 6 to pH 5, the band area is approximately constant,
398 which shows that molybdate adsorption does not modify the amount of disturbed surface
399 hydroxyls on the (010) faces. Below pH 5, a second trend appears where the doublet area is

400 diminished and reaches a plateau around pH 4. The decreasing area of the doublet can be
401 interpreted as the release of protonated hydroxyl groups in solution, which is consistent with
402 the formation of bidentate complexes.
403 Figure 7 shows the evolution of the area of the bands with increasing pH identified by the
404 curve fitting procedure. For more clarity, the bands are separated into several groups
405 (corresponding to Figures 7a) to 7d). Each figure corresponds to bands forming one cluster.
406 As shown in Figure 7a), the evolution of the 950 cm^{-1}, 935 cm^{-1} and 913 cm^{-1} bands is
407 plotted. The 950 cm^{-1} component is only observable starting from pH 5.5 and shows its
408 highest increase from pH 5.5 to pH 4.5. Its appearance during the pH decrease and its
409 observed increase is in agreement with its assignment to bidentate complexes, based on
410 observations of Figure 5. Regarding the 934 cm^{-1} band (symmetric stretching of the Mo-O
411 bonds of inner-sphere complexes), its intensity remains high over the whole pH range. The
412 913 cm^{-1} band (asymmetric stretching of the Mo-O bonds of the monodentate surface
413 complex) increases down to pH 4. A sudden increase in the number of monodentate
414 complexes takes place at pH 5, corresponding to the pH at which the bidentate complexes are
415 observed to appear and increase as indicated above. Thus, the pH-edge of the adsorption for
416 both complexes is similar, meaning that the formation of the bidentate species is associated
417 with the growth of the monodentate on the (010) faces of lepidocrocite.
418 Figure 7b depicts the evolution of the wide bands in the cluster (the large band width can
419 used as a criterion to associate the bands with outer-sphere complexes [46]). The band at 842
420 cm^{-1} is assigned to the outer-sphere complex with MoO_4^{2-}, and a possible assignment for
421 another outer-sphere complex can include $HMoO_4^-$, since the concentration of this aqueous
422 species becomes nonnegligible (its pKa is 3.8 [17]). Protonation implies a lowering of the
423 symmetry, and so a splitting, but no other wide band was observed in the spectra (perhaps
424 because of a too low intensity. Figure 7b shows that the increase in the 878 cm^{-1} band area is

425 accompanied by a decrease in the 842 cm^{-1} band area. The distribution between these two

426 bands is close to the solution speciation, even if the protonated molybdate appears to be

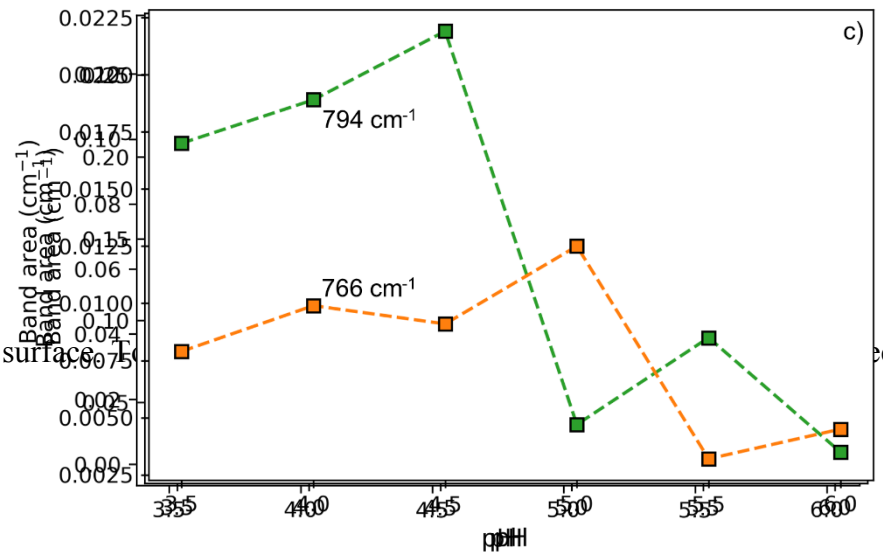

427 favored at the surface. T ecule can be

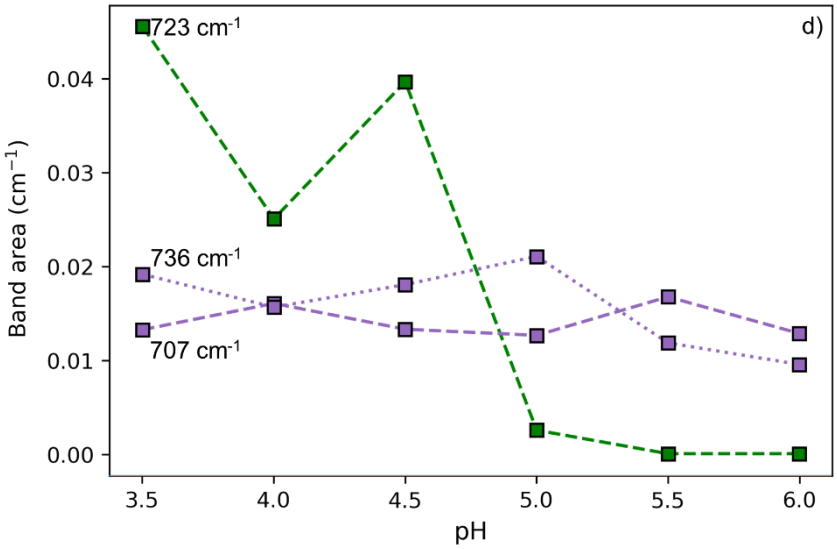

compensated for by two $HMoO_4^-$ anions in the surface vicinity, which can explain this trend.

Figure 7. Band areas for the different components separated by curve fitting with pH: a) bands at 950 cm^{-1}, 935 cm^{-1} and 919 cm^{-1}, b) bands at 878 cm^{-1} and 842 cm^{-1}, c) bands at 794 cm^{-1} and 766 cm^{-1}, and d) bands at 736 cm^{-1}, 723 cm^{-1} and 707 cm^{-1}. The lines are visual guides.

Concerning the 794 cm^{-1} band shown in Figure 7c, its area is low between pH 6 and pH 5 but then strongly increases at pH 5. This is in agreement with the behavior of the OH groups of the lepidocrocite surface (Figure 6b) and with the evolution of the 950 cm^{-1} band (Figure 7a). This result is consistent with the assignment of the 950 cm^{-1} band to symmetric stretching of a bidentate complex. The overall increase in the 766 cm^{-1} band with decreasing pH can correspond to the formation of a protonated monodentate complex. Indeed, as molybdates have a pKa of approximately 4, it is possible that the complex can be protonated.

The evolution of the 736 cm^{-1}, 723 cm^{-1}, and 707 cm^{-1} bands is shown in Figure 7d. The 736 cm^{-1} band is assigned to a monodentate complex that is particularly stable at the lepidocrocite surface, which is adsorbed on surface defects. The 707 cm^{-1} band is assigned to monodentate species close to the 736 cm^{-1} band but with different environments (e.g., H bond

445 configuration). The 723 cm^{-1} band appears at pH 5.5 and increases strongly, following the
446 trend observed for the 950 cm^{-1} and 766 cm^{-1} bands, which are assigned to bidentate
447 complexes. This band may, therefore, arise from the ν_3 band splitting associated with the
448 transition from a monodentate complex to a bidentate complex. The ν_3 band splitting then
449 becomes higher (average value of 94 cm^{-1} against 44 cm^{-1} in Figure 2c)), and this increase
450 shows that bidentate complexes are more stable than the corresponding monodentate
451 complexes (found on the "ideal" surface of the (010) faces of lepidocrocite). The curve fitting
452 results do not show any major changes in wavenumber upon pH evolution, which is
453 confirmed by the 2D spectra (Figure 5).
454
455 **3.3. Polarized ATR-IR: Insights into the substrate and adsorbate orientations**
456
457 The use of a polarized IR beam allows us to gather orientational information about the
458 samples studied by unveiling the direction of the transition dipolar moment (the change in
459 dipolar moment of a molecule upon vibration) of the system studied, whether it is a substrate
460 or an adsorbate. This allows us to obtain information about a specific face of lepidocrocite or
461 the orientation of surface complexes. This can bring support and some complementary data
462 for the interpretation of the surface speciation detailed above.
463 The first step to apply this technique is to form a film of particles with oriented surfaces.
464 Lepidocrocite particles are characterized by a large anisotropy with a lath-shaped morphology
465 (Figure S1); stacking these particles can ideally lead to the formation of a layer with most of
466 the particles laid flat with the (010) face parallel to the ATR crystal surface. However, once
467 this deposit comes into contact with a solution, electric charge builds up at the surface,
468 leading to a possible repulsion between particles and a change in the particle packing. This
469 charge build-up results from (de)protonation of surface hydroxyl groups and the presence of

inner-sphere surface complexes. According to DLVO theory, this could be the case if the Coulombian term prevailed in the van der Waals term [47]. To evaluate the extent of this phenomenon, which can decrease the "quality" of the deposit and lead to difficulties in the interpretation of the spectra, the evolution of the particle orientation in the deposit ((A_z, A_y) diagrams) was followed during a change in pH (Figure 8a)) and with (Figure 8b)) or without an adsorbate.

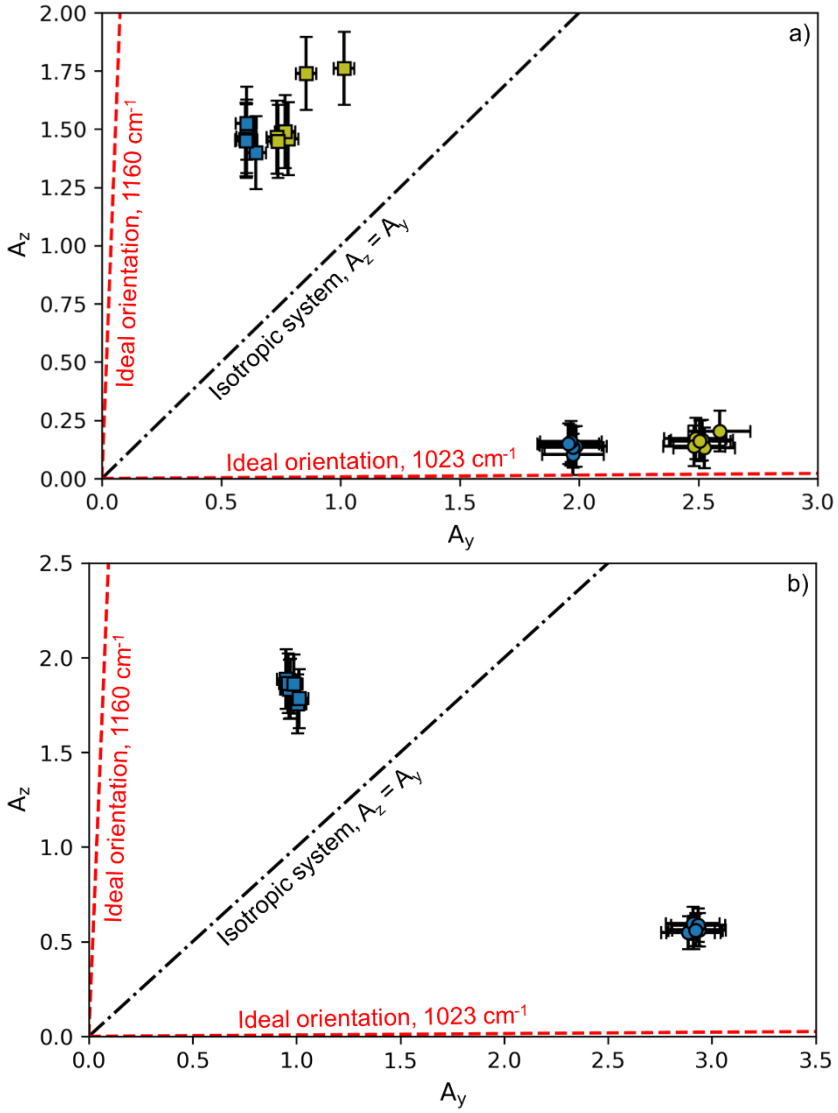

Figure 8: (A_z, A_y) diagram for lepidocrocite particle films for the 1160 cm^{-1} band (squares) and 1023 cm^{-1} band (circles): a) in contact with aqueous solutions of different pH values (between 3 and 10) and b) in contact with aqueous solutions of molybdates (10^{-4} mol. L^{-1}) at

480 several pH values (between 6 and 3.5). The pH is not specified for each point, as most of the
481 values are inside the error bars. The red dashed lines represent the ideal values determined by
482 DFT calculations performed on bulk lepidocrocite, and the black dash-dotted line corresponds
483 to an anisotropic packing of the particles. It is worth noting that lepidocrocite bending modes
484 do not show important changes between dried and hydrated deposits, making this
485 computational result relevant for comparison. The blue and yellow points correspond to two
486 different experiments

487

488 The area of the A_y and A_z components of the 1160 cm^{-1} and 1020 cm^{-1} IR bands were
489 measured for different pH values (from 10 to 3, Figure 8a). Both bands correspond to FeOH
490 bending, but for the 1020 cm^{-1} band, the transition dipolar moment is parallel to the (010)
491 face, while for the 1160 cm^{-1} band, the transition dipolar moment is oriented almost
492 perpendicular to the (010) face. This corresponds to the theoretical value of A_z being equal to
493 zero for 1020 cm^{-1} and a line that is almost vertical near the A_z axis for 1160 cm^{-1} [37]. The
494 experimental results are characterized by a strong dichroism ($A_y \neq A_z$), although it is not as
495 strong as the theoretical predictions.

496 Regardless of the pH value, the lepidocrocite particle packing is the same within the
497 packing error. This error is defined as the standard deviation of the (A_z, A_y) points calculated
498 on the basis of 36 measurements on dried deposits. This result was found to be reproducible
499 and to not rely on the pH value sequence. Contacting the dry deposit with solutions of
500 different compositions did not lead to a strong perturbation of the stacking, confirming that
501 van der Waals forces prevail on the electrostatic forces in this kind of system. Once packed,
502 the particles can no longer be separated regardless of their surface charge. Such observations
503 agree with other research work on the same substrate [48] showing that lepidocrocite particles
504 tend to aggregate on the (010) faces, which are characterized by a low surface charge with

respect to other crystallographic faces. The main difference from those results is that the time taken to obtain such an aggregation degree (one-year time-scale) is reduced thanks to the drying of the suspension. The present work highlights the potential of polarized ATR-IR (pATR-IR) spectroscopy as a suitable analytical technique to study the packing of nanoparticles in a film.

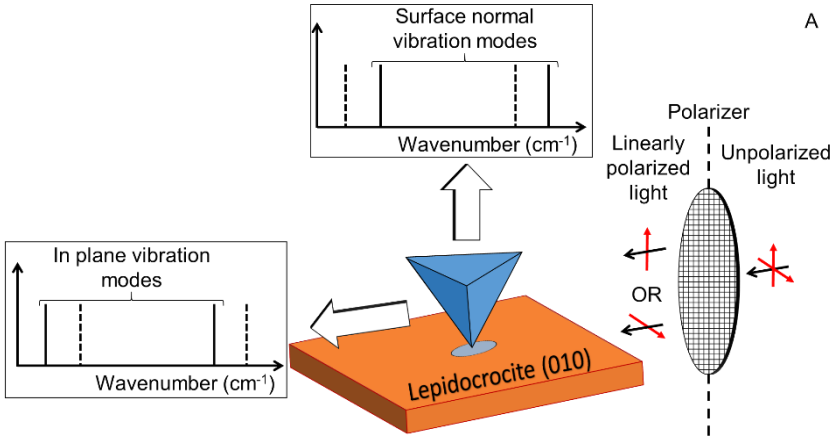

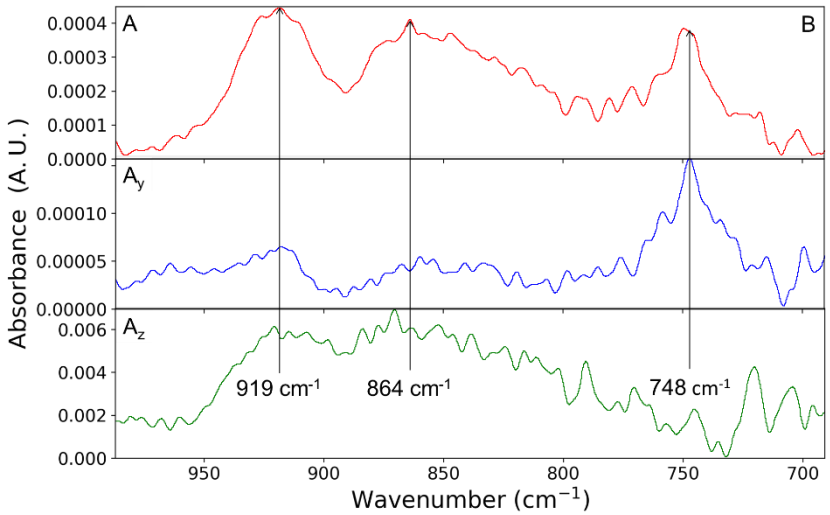

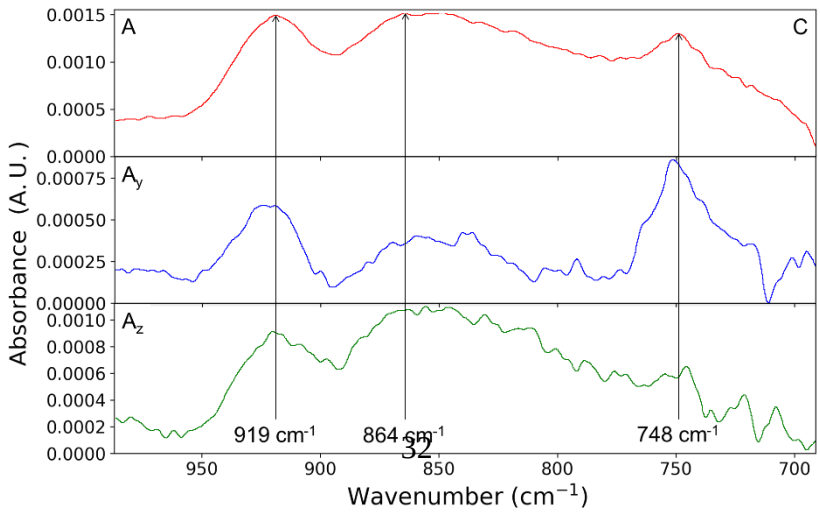

Figure 9: (A) Diagram of a monodentate complex and its associated spectra with linearly polarized light oriented along the plane and perpendicularly to it. A(top), A_y(middle) and A_z(bottom) spectra for the molybdate wavenumber region at 4.10^{-4} mol. L^{-1} (B) and 10^{-3} mol. L^{-1} (C) in molybdates at pH 8. The vertical arrows show the major signals observed in the spectra.

Figure 9 shows the spectra measured for the adsorbed molybdate ions with unpolarized radiation and for the A_y and A_z components of the absorbance. Two different concentrations were used (4.10^{-5} mol/L and 10^{-3} mol/L) at pH 8, and this large difference illustrates the impact of the surface coverage on the packing order. From a geometrical point of view, a tetrahedral oxo-anion in a monodentate complex is characterized by a C_{3v} symmetry, leading to three nondegenerate stretching modes: a symmetric mode and two asymmetric modes (called $\nu_3(E)$ and $\nu_3(A_1)$ [49]). Among the two asymmetric vibration modes of a monodentate complex, $\nu_3(A_1)$ has its transition dipolar moment oriented along the surface normal as $\nu_3(E)$ has its transition dipolar moment oriented perpendicularly to the surface normal. If the surface normal corresponds to the z-axis, such a surface structure should be observed as an IR band with an A_z contribution only. For the case of the latter vibration mode, only a A_y contribution should be observed. This is depicted in Figure 9A. The situation is different for a bidentate complex: this surface complex belongs to the C_{2v} group of symmetry and is characterized by four stretching modes. Two of these modes due to symmetric stretching of the Mo-O bonds have a transition moment collinear to the surface normal. However, the two other asymmetric stretching modes have their associated transition moment orthogonal to the surface's normal. Consequently, for such a complex, two bands should be observed on A_z and two on A_y.

The band present at approximately 919 cm^{-1}, visible on A_y, appears to be present among other bands on the A_z component, which can explain the wide band observed. The 864 cm^{-1} band is almost invisible on the A_y component but is far more visible and wider on A_z. The band centered at ca. 748 cm^{-1} is not found on the A_z component but is clearly present on the A_y component. The several smaller bands observed on the A_y component at 919 cm^{-1} and the wide band at 864 cm^{-1} suggest that different surface species are present or that the disorder in the particle film creates deviations with respect to an ideally oriented system. If the atypical (defect) inner-sphere complex nature is considered, the mononuclear monodentate complex is already slightly tilted on the surface because of the sp^3 hybridization of the oxygen atom interacting with the surface. As a result, each vibration mode has a nonzero value for its A_y and A_z components, which directs the interpretation toward an expected behavior where the low intensity bands observed in Figure 9B arise from the atypical surface complex, which would be of the mononuclear monodentate type. The intensity differences can then indicate surface density differences between surface species. Thus, the complex assigned to the 748 cm^{-1} band has a higher surface density than the other complex, presenting a lower intensity.

As shown in Figure 9C, the bands continue to increase and are as visible as in the unpolarized spectrum. The peak at 919 cm^{-1} is observed for both A_y and A_z because of the strong overlap between the ν_1 and ν_3 bands [31]. This is in agreement with the secondary adsorption of typical (and less reactive) molybdate on “ideal” (010) environments at the lepidocrocite surface.

Furthermore, the order of the wavenumber between the $\nu_3(E)$ and $\nu_3(A_1)$ bands is reversed between the two complexes. The difference between adsorption modes (mononuclear monodentate or monodentate) or the chemical environment of the complexes can provide

562 these changes. These results indicate that pATR-IR spectroscopy enables surface complex
563 characterization but also enables deeper analysis by separation of the different asymmetric
564 stretching modes.

565 Linear polarization of the IR beam was also used to spectroscopically study the
566 molybdate/lepidocrocite system at a molybdate concentration of 10^{-4} mol. L^{-1} and an NaCl
567 ionic strength of 0.01 mol. L^{-1} for different pH values (6 to 3.5, Figure 10).

568 As shown in the unpolarized spectrum, three major bands are observed at approximately
569 927 cm^{-1}, 873 cm^{-1} and 736 cm^{-1}. These bands are also found in the A_z and A_y components of
570 the absorbance but with different intensities and morphologies. This indicates that the surface
571 environments, for the experimental conditions used, are more diverse than in the previous
572 experiment performed at a higher pH (Figures 9B and C). The 736 cm^{-1} band is predominant
573 on A_z and has a bathochromic shoulder, which indicates that two vibration modes have their
574 respective transition moment coplanar to the normal of the (010) facets of lepidocrocite. The
575 higher intensity of this band in the A_z component with respect to the A_y component is
576 different from that observed in Figures 9B and C. The bands observed at approximately 927
577 and approximately 873 cm^{-1} prevail in intensity for the A_y component of the absorbance. For
578 the previous experiment, it is expected that the 927 cm^{-1} band arises from two overlapping
579 vibration modes of the monodentate (or monodentate mononuclear) complexes (ν_1 et $\nu_3(A_1)$)
580 for which the transition moments are oriented in the same direction. However, these would be
581 predominantly oriented toward the z-axis at pH 8, and their situation reversed here. Such a
582 difference between the A_y and A_z components can be explained by having monodentate
583 complexes tilted toward the surface, most likely due to interaction with neighboring OH
584 groups (hydrogen bonding)[31]. In this way, the transition moments of the ν_1 and $\nu_3(A_1)$
585 vibration modes will show increasing xy components while their z components show a
586 decrease. The reverse is equally true for the $\nu_3(E)$ mode, and the associated transition moment

direction is taken as being parallel to the surface. No major signal is observed at approximately 927 cm^{-1} or 873 cm^{-1} in Figure 10a for the A_z component. However, such signals are present in Figure 10c, which confirms the hypothesis that the monodentate (or mononuclear monodentate) complexes are tilted toward the surface when they are protonated. The weaker absorbance of A_z with respect to A_y can arise from the correction of the baseline, which can slightly truncate the intensities of the spectra (Figure 10c). Additionally, the weak surface fractions of other exposed faces enable the specific characterization of the (010) faces and the corresponding adsorption, but the molybdates can also adsorb onto other facets. These sorbed species on minor facets can express themselves with small intensities in the spectra shown in Figures 9B and C.

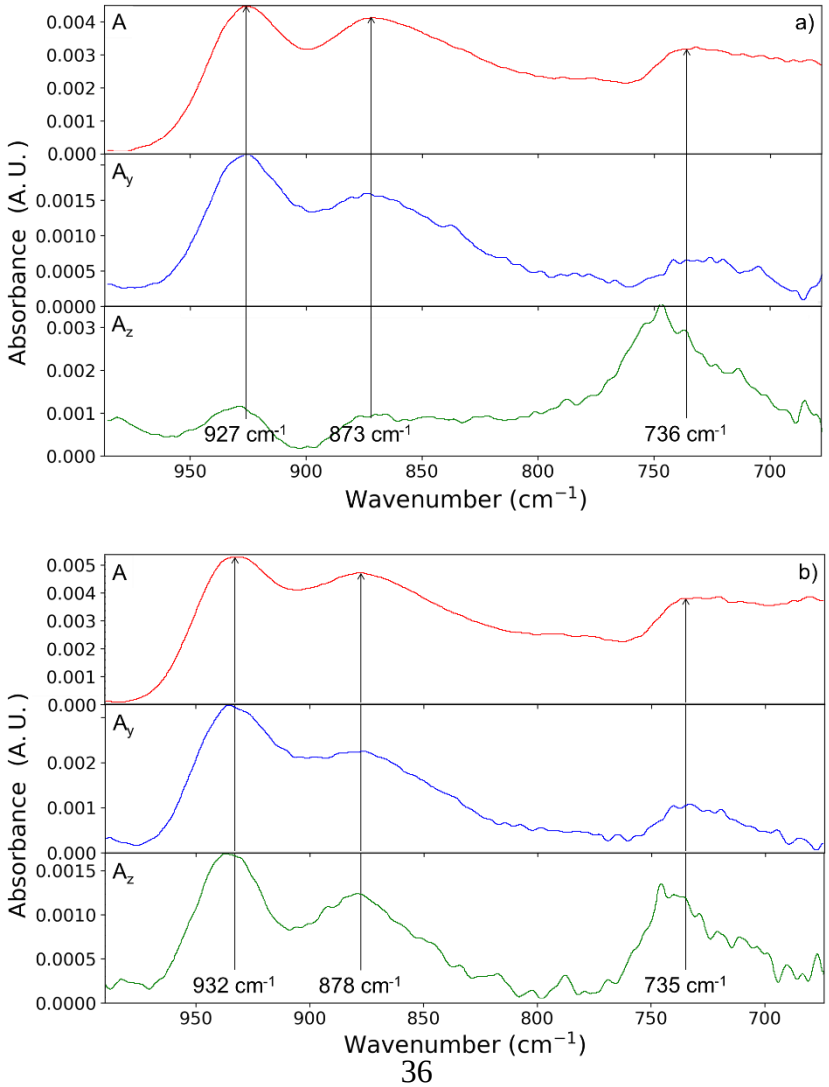

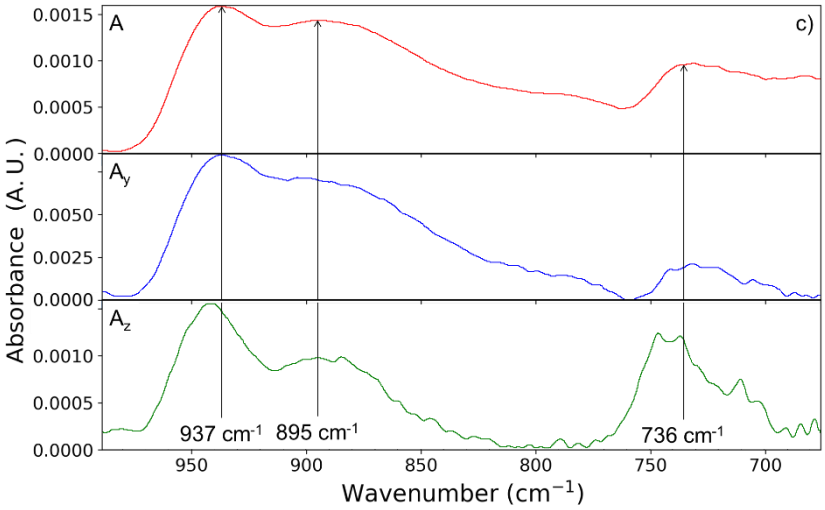

Figure 10: A(top), A_y(middle) and A_z(bottom) spectra for the molybdate wavenumber region at a) pH 6, b) pH 5 and c) pH 4. The vertical arrows indicate the major bands observed in the spectra.

As shown in Figure 10, between the cluster of bands observed at 873 cm^{-1} and that at approximately 736 $cm^{-1,}$ no signal on A_z is visible, but a shoulder is present on A_y. As demonstrated by the clear contrast between A_z and A_y for this vibration mode, the corresponding transition moment must be strictly parallel to the surface. The surface species closest to this description is the bidentate complex because it is strongly anchored to the surface and does not have any mobility about its adsorption site at the surface. This interpretation is in agreement with that made in the study of the unpolarized spectra for the same system. As shown in Figure 10, a large band at approximately 735 cm^{-1} is visible on A_z. It is nontrivial to determine whether this feature arises from an orientational defect of the monodentate (or mononuclear monodentate) complexes, for which the vibration modes show a clear orientation along the z-axis, or from another vibration mode of the bidentate

617 complexes, as previously determined without the help of polarized light. From a global point
618 of view, the decrease in pH, from pH 6 to pH 4, does not appear to modify the orientation of
619 the surface complexes; it is rather the band intensity (on A_z and A_y) that is increased. This
620 increase without any major modification of the spectra/morphology points toward the fact that
621 each newly adsorbed complex has a new configuration (tilted by H bond) detailed herein.
622

4. Conclusion

In this work, the adsorption of molybdates on lepidocrocite was studied by infrared in situ spectroscopy, with and without polarization. First, the solid/solution interface at pH 8 was studied, and the concentration of molybdate anions was modified over a wide range (10^{-5} to 10^{-3} mol/L). The results enabled us to reveal the existence of a 748 cm^{-1} band, which has not been reported in previous works. This band can be assigned to a second molybdate species adsorbed on the lepidocrocite surface. This new species shows an IR signal that is consistent with a molybdate adsorbed as a monodentate complex on surface defects of (010) facets, which are the major surfaces exposed for the studied substrate. The other surface species, already noted in the literature, are assigned to monodentate complexes. Previous works for this system enabled us to assign all the vibration modes on the basis of the observed shoulders. The analysis of the hydroxyl deformation bands for lepidocrocite confirmed that the major facets for adsorption are indeed (010) facets. A curve fitting procedure was performed to hone the IR band assignment, which confirmed the previous assignment for the raw spectra and highlighted the weak adsorption site density. An outer-sphere complex was also revealed by curve fitting.

The study of the pH influence on molybdate surface speciation, and in particular for the newly found band at 748 cm^{-1}, was carried out, which showed a major change in the spectral intensity as well as the spectral shape between pH 8 and pH 6. The appearance of a bathochromic shoulder, in association with DFT calculations from the literature, enabled us to propose the existence of bidentate complexes at the lepidocrocite surface. The lone band at 748 cm^{-1} at pH 8 becomes a band cluster at pH 6, and such variation continues to be observed throughout the whole pH range, which has never been described before. A deconvolution of the spectra based on Gaussian curves was performed to assign the different bands composing

the observed band clusters. Although some bands were not found at pH 6 despite the fact they exist at pH 8, an assignment was made that showed the existence of binuclear monodentate complexes, justifying the low reactivity of the (010) facets, bidentate complexes arising from the rearrangement of monodentate complexes at low pH values, and also protonated monodentate complexes on the surface, which are probably adsorbed on "classical" adsorption sites of well crystallized, defect-free domains. Two outer-sphere complexes were also found thanks to the curve fitting procedure. These complexes were assigned to unprotonated (MoO_4^{2-}) and monoprotonated ($HMoO_4^-$) species. The curve fit also enabled us to show the high affinity of the bidentate complexes for the (010) "ideal" facets of lepidocrocite on the basis of the component's band area for the band cluster at approximately 752 cm^{-1}. The curve fitting procedure did not show any major changes in wavenumber upon pH evolution, which was confirmed by 2D correlation IR analysis.

These results show that even a simple adsorbate/substrate system shows complexity that can be extensively described using only a combined spectroscopic approach. This work illustrates how the use of in situ ATR-IR spectroscopy can still progress to bring an increasingly refined view of solid–solution interfaces.

Acknowledgments

The authors thank the Collège de France for providing the lepidocrocite samples as well as the doctoral school ED388 for supporting R. Botella in his research. Dominique Costa (IRCP) is thanked for the fruitful discussions on surface modeling.

References

[1] McQuillan, A., J. Probing Solid-Solution Interfacial Chemistry with ATR-IR Spectroscopy of Particle Films. *J. Adv. Mater.* 2001, 13, 1034-1038

[2] Gustafsson, J., P. Modelling molybdates and tungstate adsorption to ferrihydrite. *Chem. Geol.* 2003, 200, 105-115

[3] Rietra, R., P., J., J.; Hiemstra, T.; Van Riemsdijk, W., H. The relationship between molecular structure and ion adsorption on variable charge minerals. *Geochim. Cosmochim. Acta* 1999, 63, 3009-3015

[4] Peak, D.; Ford, R.; Sparks, D., L. An in Situ ATR-FTIR Investigation of Sulfate Bonding Mechanisms on Goethite. *J. Colloid. Interface Sci.* 1999, 218, 289-299

[5]Wijnja, H.; Schulthess, C., P. Vibrational Spectroscopy Study of Selenate and Sulfate Adsorption Mechanisms on Fe and Al (Hydr)oxide Surfaces. *J. Colloid. Interface Sci.* 2000, 229, 286-297

[6] Vissenberg, M., J.; Joosten, L., J., M.; Heffels, M., M., E., H.; van Welsenes, A., J.; San de Beer, V., H., J.; van Santen, R., A.; Rob van Veen, J., A. Tungstate versus Molybdate Adsorption on Oxidic Surfaces: A Chemical Approach. *J. Phys. Chem. B* 2000, 104, 8456-8461

689 [7] Bostick, B., C.; Sun, J.; Landis, J., D.; Clausen, J., L. Tungsten Speciation and Solubility
690 in Munitions-Impacted Soils. *Environ. Sci. Technol.* 2018, 52, 1045-1053

691 [8] Xu, N.; Braida, W.; Christodoulatos, C.; Chen, J. A Review of Molybdenum Adsorption
692 in Soils/Bed Sediments: Speciation, Mechanism and Model Applications. *Soil Sediment*
693 *Contam.* 2013, 22, 912-929

694 [9] Das, S.; Hendry, M., J. Adsorption of molybdate by synthetic hematite under alkaline
695 conditions: Effects of aging. *Appl. Geochem.* 2013, 28, 194-201

696 [10] Otte, K.; Schmahl, W. ; Pentcheva, R. DFT+U Study of Arsenate Adsorption on
697 FeOOH Surfaces: Evidence for Competing Binding Mechanisms. *J. Phys. Chem. C* 2013,
698 117, 15571-15582

699 [11] Lefèvre, G. In situ Fourier-transform infrared spectroscopy studies of inorganic ions
700 adsorption on metal oxides and hydroxides. *Adv. Colloid Interfac.* 2004, 107, 109-123

701 [12] June, D.; Franses, E., I. Orientations of Chain Axes and Transition Moments in
702 Langmuir-Blodgett Monolayers Determined by Polarized FTIR-ATR Spectroscopy. *J.Phys.*
703 *Chem.* 1992, 96, 9952-9959

704 [13] Holmgren, A.; Yang, X. A Polarized Fourier Transform Infrared Spectrometry
705 Attenuated Total Reflection Study of Bentonite Settled onto Magnetite. *J. Phys. Chem. C*
706 2008, 112, 16609-16615

707 [14] Davantès, A.; Lefèvre, G. Molecular orientation of molybdate ions adsorbed on
708 goethite nanoparticles revealed by polarized in situ ATR-IR spectroscopy. *Surf. Sci.* 2016,
709 653, 88-91

[15] Davantès, A.; Lefèvre, G. In Situ characterization of (poly)molybdate and (poly)tungstate ions sorbed onto iron (hydr)oxides by ATR-FTIR spectroscopy. *Eur. Phys. J.-Spec. Top.* 2015, 224, 1977-1983

[16] Boily, J.-F.; Kozin, P., A. Particle morphological and roughness controls on mineral surface charge development. *Geochim. Cosmochim. Acta* 2014, 141, 567-578

[17] Tytko, K., H. Structure, bonding and acid-base properties of protonated monometalate ions and polymetalate ions forming chains or rings of corner-sharing mo_4 tetrahedra of transition metals of groups v and vi - a theoretical approach. *Polyhedron* 1986, 8, 497-503

[18] Schwertmann, U.; Cornell, R. M. Iron Oxides in the Laboratory: Preparation and Characterization, 2nd ed.; VCH: 2000.

[19] Pedley, M. E.; Davies, P. B. A polarized ATR study of structural orientation in dry and humid thin HPMC films. *Vib. Spectrosc.* 2009, 49, 229−236.

[20] Ras, R. H. A.; Schoonheydt, R. A.; Johnston, C. T. Relation between s-Polarized and p-Polarized Internal Reflection Spectra: Application for the Spectral Resolution of Perpendicular Vibrational Modes. *J. Phys. Chem. A* 2007, 111 (36), 8787−8791.

[21] Morita, S. *2DShige;* Kwansei-Gakuin University, 2004-2005.

[22] Gericke, A.; Gadaleta, S., J.; Brauner, J., W.; Mendelsohn, R. Characterization of biological samples by tzo-dimensional infrared spectroscopy: Simulation of frequency, bandwidth, and intensity changes. *Biospectroscopy* 1996, 2, 341-351

[23] Kresse, G.; Hafner, J. Ab initio molecular dynamics simulation of the liquid-metal-amorphous-semiconductor transition in germanium. *Phys. Rev. B* 1994, *49*, 14251–14269

731 [24] Kresse, G.; Joubert, D. From ultrasoft pseudopotentials to the projector augmented-
732 wave method. *Phys. Rev. B* 1999, 59, 1758–1775

733 [25] Perdew, J. P.; Burke, K.; Ernzerhof, M. Generalized Gradient Approximation Made
734 Simple. *Phys. Rev. Lett.* 1996, 77, 3865–3868

735 [26] Grimme, S. Semiempirical GGA-type density functional constructed with a long-range
736 dispersion correction. *J. Comput. Chem.* 2006, 27, 1787-1799

737 [27] Guo, H.; Barnard, A., S. Modeling the iron oxides and oxyhydroxides for the
738 prediction of environmentally sensitive phase transformations. *Phys. Rev. B*: *Condens. Matter*
739 *Mater. Phys.* 2011, 83, 094112

740 [28] Pinney, N.; Kubicki, J., D.; Middlemiss, D., S.; Grey, C., P.; Morgan, D. Density
741 Functional Theory Study of Ferrihydrite and Related Fe-Oxyhydroxides. *Chem. Mater.* 2009,
742 21, 5727-5742

743 [29] Christensen, H.; Christensen, A., N. Hydrogen bonds of gamma-FeOOH. *Acta Chem.*
744 *Scand., Ser. A* 1978, 32, 87-88

745 [30] Karhanek, D. Self-Assembled Monolayers Studied by Density-Functional Theory.
746 Ph.D.,Wien Universität, Wien, 2010

747 [31] Davantès, A.; Costa, D.; Lefèvre, G. Molybdenum(VI) Adsorption onto Lepidocrocite
748 (γ-FeOOH): In Situ Vibrational Spectroscopy and DFT+U Theoretical Study. *J. Phys. Chem.*
749 *C* 2016, 120, 11871-11881

750 [32] Frost, R., L.; Musumeci, A., W.; Martens, W., N.; Adebajo, M., O.; Bouzaid, J.
751 (Raman spectroscopy of hydrotalcites with sulphate, molybdate and chromate in the
752 interlayer. *J. Raman Spectrosc.* 2005, 36, 925-931

[33] Davantès, A. Apport de la spectroscopie infra-rouge in situ à l'étude des réactions de complexation à l'interface solide/solution. Ph.D., Université Pierre et Marie Curie, Paris, Sept. 2015

[34] Davantès, A.; Costa, D.; Sallman, B.; Rakshit, S.; Lefèvre, G. Infrared Study of (Poly)tungstate Ions in Solution and Sorbed into Layered Double Hydroxides: Vibrational Calculations and In Situ Analysis. *J. Phys. Chem. C* 2017, 121, 324−332

[35] Sing, K., S., W.; Everett, D., H.; Haul, R., A., W.; Moscou, L.; Pierotti, R., A.; Rouquérol, J.; Siemieniewska, T. Reporting physisorption data for gas/solid systems with special reference to the determination of surface area and porosity. *Pure Appl. Chem.* 1985, 57, 4, 603-619

[36] Giles, C., H.; Smith, D. A General Treatment and Classification of the Solute Adsorption Isotherm: I. Theoretical. *J. Colloid Interface Sci.* 1974, 47, 755-765

[37] Weckler, B.; Lutz, H., D. Lattice vibration spectra. Part XCV. Infrared spectroscopic studies on the iron oxide hydroxides goethite (alpha), akaganeite (beta), lepidocrocite (gamma), and feroxyhite (delta). *Eur. J. Sol. State Inor.* 1998, 35, 531-544

[38] Lewis, D., G.; Farmer, V., C. Infrared Absorption Of Surface Hydroxyl Groups And Lattice Vibrations In Lepidocrocite (Gamma-FeOOH) And Boehmite (Gamma-AlOOH). *Clay Miner.* 1986, 21, 93-100

[39] Hiemstra, T.; Van Riemsdijk, W., H. Adsorption and surface oxidation of Fe(II) on metal (hydr)oxides. *Geochim. Cosmochim. Acta* 2007, 71, 5913-5933

[40] Ritzhaupt, G.; Devlin, J., P. Infrared spectra of matrix isolated alkali metal perchlorate ion pairs. *J. Chem. Phys.* 1975, 62, 1982-1986

775 [41] Kallay, N.; Zalac, S. Charged Surfaces and Interfacial Ions. *J. Colloid Interface Sci.*
776 2000, 230, 1-111

777 [42] Hug. S. J.; Bahnemann, D., J. Infrared spectra of oxalate, malonate and succinate
778 adsorbed on the aqueous surface of rutile, anatase and lepidocrocite measured with in situ
779 ATR-FTIR *J. Electron Spectrosc.* **2006**, 150, 208-219

780 [43] Wan, J.; Simon, S.; Deluchat, V.; Dictor, M.-C.; Dagot, C. Adsorption of AsIII, AsV
781 and dimethylarsinic acid onto synthesized lepidocrocite *J. Environ. Sci. Heal. A* **2003**, 48,
782 1272-1279

783 [44] Noda I. and Ozaki Y. (2004) *Two-Dimensional Correlation Spectroscopy. Applications in*
784 *Vibrational and Optical Spectroscopy,* John Wiley Inc, NY.

785 [45] Huang, H.; Xie, J.; Chen, H. Adsorption behavior of human serum albumin on ATR
786 crystal studied by in situ ATR/FTIR spectroscopy and two-dimensional correlation analysis.
787 *Analyst* 2011, 136, 1747-1752

788 [46] Lefèvre, G.; Fédoroff, M. Sorption of sulfate ions onto hematite studied by attenuated
789 total reflection-infrared spectroscopy: Kinetics and competition with other ions. *Phys. Chem.*
790 *Earth* 2006, 31, 499-504

791 [47] Trefalt, G.; Ruiz-Cabello, F., J., M.; Borkovec, M. Interaction Forces,
792 Heteroaggregation, and Deposition Involving Charged Colloidal Particles. *J. Phys. Chem. B*
793 2014, 118, 6346-6355

794 [48] Kozin, P., A.; Salazar-Alvarez, G.; Boily, J.-F. Oriented Aggregation of Lepidocrocite
795 and Impact on Surface Charge Development. *Langmuir* 2014, 30, 9017-9021

796 [49] Laane, J.; Ocola, E., J. Applications of Symmetry and Group Theory for the
797 Investigation of Molecular Vibrations *Acta Appl. Math.* **2012**, 118, 3-24